Analysis of Flow Factor Control Strategy in Vanadium Redox Flow Batteries

Sergei Parsegov, Mikhail Pugach, Andrey Polyakov, Federico Ibáñez

Analysis of Flow Factor Control Strategy in Vanadium Redox Flow Batteries

Sergei Parsegov * **Mikhail Pugach** * **Andrey Polyakov** ** **Federico Ibáñez** *

* *Skolkovo Institute of Science and Technology, Moscow, Russia (e-mail: s.parsegov@skoltech.ru, m.pugach@skoltech.ru, fm.ibanez@skoltech.ru, p.vorobev@skoltech.ru)*
** *Inria Lille-Nord Europe, Lille, France (e-mail: andrey.polyakov@inria.fr)*

Abstract: Optimization of the performance of vanadium redox flow batteries (VRFBs) is closely related to flow rate control: a proper flow rate adjustment reduces the losses and extends the battery lifetime. In this regard, the so-called flow factor control strategy of VRFBs has been recently proposed in the literature and some numerical/experimental validations have been performed. The strategy is a generalization of Faraday's first law of electrolysis as it uses a special scaling parameter referred to as the *flow factor*. In our paper, we show how this factor is related to the *conversion rate* (fraction conversion per pass) and geometrical properties of the battery. Finally, we investigate the flow factor as a function of the fraction conversion per pass and stack/tank volumes, and perform numerical simulations to confirm the theoretical results.

Keywords: flow rate control, vanadium redox flow battery, flow factor.

1. INTRODUCTION

Batteries are the key technology for the sustainable development of electrical grids with a high share of renewable power generation, e.g. see Lucas and Chondrogiannis (2016). Among different battery technologies, Vanadium Redox Flow Batteries (VRFBs) are considered to be one of the most promising solutions for large-scale energy storages suitable for integration with renewables due to their good scalability and long cycling life, see Aneke and Wang (2016); Viswanathan et al. (2014). VRFB uses electrolytes stored in two separated tanks and pumped though the cells where electrochemical conversion takes place, e.g. see Pugach et al. (2017). As a result, energy and power ratings of VRFB systems are decoupled: applications requiring more energy only need larger volumes of the electrolytes, while more power can be obtained by adding more electrochemical cells, see Pugach et al. (2019).

To maintain permanent conversion in the cell, the electrolytes should be pumped with the proper flow rate, that assures supply of fresh active ions taking place in the electrochemical reactions, see Faraday (1834). Therefore, control of electrolyte flow rate is one of the most import issues during VRFB operation, see Trovò et al. (2021). In fact, insufficient flow rate can result in poor battery performance or even in battery faults, see Pugach et al. (2020). The pioneering work devoted to this issues was performed by the group of Skyllas-Kazacos, see Largent et al. (1993), where they proposed to regulate the flow rate by switching on/off the pumps. After that, a number of studies investigated different strategies for flow rate regulation, such as sliding mode, see Ling et al. (2015), model predictive approach, see Shen et al. (2013), energy losses minimization based control, see Konig et al. (2016); Averbukh et al. (2017); Li et al. (2017b), PI-controllers, see Li et al. (2017a); Pugach et al. (2020), and fuzzy logic controllers, see Badrinarayanan et al. (2017). However, the most common approach applied for regulation of flow rate in industrial-scale VRFBs is based on Faraday's law, see Trovò (2020), that assures a minimum flow rate required for continuous reaction process (or stoichiometric flow rate), see Blanc and Rufer (2008). Konig et al. (2015) applied Faraday's law for determination of flow rate that was further used for optimal design with desired electrolyte distribution in the large-scale VRFB system. It was shown by Tang et al. (2014), that application of Faraday's law with flow factor (or stoichiometric factor) can significantly improve battery performance and that a flow factor of 7.5 allows reducing pumps consumption by 2 times.

After that, it was revealed that variable flow factor can further improve battery energy performance by increasing its energy efficiency nearly by 8% in comparison to the fixed flow factor of 1, see Kim et al. (2018). Guarnieri et al. (2020) have recently proposed a variable flow factor control of electrolyte flow rate in industrial-scale VRFB, indicating that it improves the round-trip energy efficiency of the battery by 2%. Recently such approach was applied for improvement of large-scale systems operation reducing the transport delay between the pumps and stack and improving the electrolyte distribution between the stacks in the module, see Chen et al. (2019). Xiao and Tan (2019) proposed to modify Faraday's law approximating it with power law dependent on the state of charge (SoC). They showed that such strategy allows improving the total energy efficiency by 3.5 % as compared to the constant flow rate strategy.

It should be noted, that despite the notable effort devoted to investigation of flow factor there is no clear understanding how it is related to the parameters of the real VRFB system. All studies considered above only proposed some empirical values of flow factor for their specific systems and thus, these data are hard to be extrapolated to other VRFB setups.

In this study, we analyzed the flow factor control strategy and derived how the flow factor depends on parameters of the VRFB system and desired conversion rate. The results of this research can be easily applied to any battery once the basic parameters are known. Such a mathematical expression shades a light on the flow rate regulation in the practical batteries and can be very important for development of battery management system for industrial-scale VRFB systems.

2. PROBLEM STATEMENT

2.1 VRFB Dynamical Model

The conventional scheme of the VRFB is presented in Fig. 1. Electrical energy is stored in electrolytes in two separate tanks, each tank has a volume V_{tk}. The electrolyte contains salts of vanadium dissolved in solutions of sulphuric acid. During the operation, the solutions are pumped into the cell of a volume V_c, where electrochemical conversion takes place:

Negative electrode: $V^{3+} + e^- \leftrightarrow V^{2+}$,

Positive electrode: $VO^{2+} + H_2O \leftrightarrow VO_2^+ + 2H^+ + e^-$.

The corresponding dynamics of the vanadium ion concentrations in the tanks and cells of the battery can be represented by the 8th-order system of nonlinear differential equations; the state space description of the system with n_c cells in the stack has the following form

$$\dot{\xi} = u\mathcal{A}\xi + \mathcal{J}\xi + \mathcal{D}w. \tag{1}$$

Here, vector $\xi \in \mathbb{R}^8_+$ denotes the state vector

$$\xi = [c_2^{tk}\ c_3^{tk}\ c_4^{tk}\ c_5^{tk}\ c_2^c\ c_3^c\ c_4^c\ c_5^c]^\top,$$

where c_2, c_3, c_4, and c_5 are concentrations of the corresponding ions in the tanks and cells, $u \in \mathbb{R}_+$ is the control input (flow rate), and $w \in \mathbb{R}$ stands for the measured disturbance (current). The matrices are

$$\mathcal{A} = \begin{bmatrix} -\alpha & \alpha \\ \beta & -\beta \end{bmatrix} \otimes \mathbf{I}_4, \tag{2}$$

$$\mathcal{J} = \begin{bmatrix} 0 & 0 \\ 0 & 1 \end{bmatrix} \otimes \begin{bmatrix} -J_2 & 0 & -J_4 & -2J_5 \\ 0 & -J_3 & 2J_4 & 3J_5 \\ 3J_2 & 2J_3 & -J_4 & 0 \\ -2J_2 & -J_3 & 0 & -J_5 \end{bmatrix}, \tag{3}$$

$$\mathcal{D} = [\,0\ \ 0\ \ 0\ \ 0\ \ d\ -d\ -d\ \ d]^\top, \tag{4}$$

where $\mathbf{I}_4 \in \mathbb{R}^{4\times4}$ denotes the identity matrix, $\alpha = 1/V_{tk}$, $\beta = 1/(n_cV_c)$, and $d = 1/(FV_c)$. Here, $\otimes$ denotes the Kronecker product. The volume of the tank V_{tk} is greater than the volume of the stack $V_{st} = n_cV_c$, therefore $\alpha < \beta$.

The matrix $\mathcal{J}$ stands for the crossover parasitic dynamics, and its entries J_2, J_3, J_4, J_5 are assumed to be either known constants, see Tang et al. (2011) or known functions of the current w, see Pugach et al. (2018).

The following algebraic constraints hold:

$$\xi_1 + \xi_2 + \xi_3 + \xi_4 = 2c_\mathrm{b}, \tag{5}$$

$$\xi_5 + \xi_6 + \xi_7 + \xi_8 = 2c_\mathrm{b}, \tag{6}$$

where c_b denotes constant total concentration which is known.

The outputs y_in, y_out of system (1) correspond to inlet (OCV_{in}) and outlet (OCV_{out}) voltages of open circuit cells, respectively (see Fig. 1) and have the form

$$y_\mathrm{in} = y_0 + y_1 \ln \frac{\xi_1\xi_4}{\xi_2\xi_3}, \tag{7}$$

$$y_\mathrm{out} = y_0 + y_1 \ln \frac{\xi_5\xi_8}{\xi_6\xi_7}, \tag{8}$$

where y_0 is a standard electrode potential and $y_1 = \frac{RT}{F}$, both are known constants; $R = 8.314\ \frac{J}{K\,\mathrm{mol}}$ is the gas constant, $F = 96485.332\ \frac{C}{\mathrm{mol}}$ is the Faraday constant, and $T = 298\ K$ is the temperature.

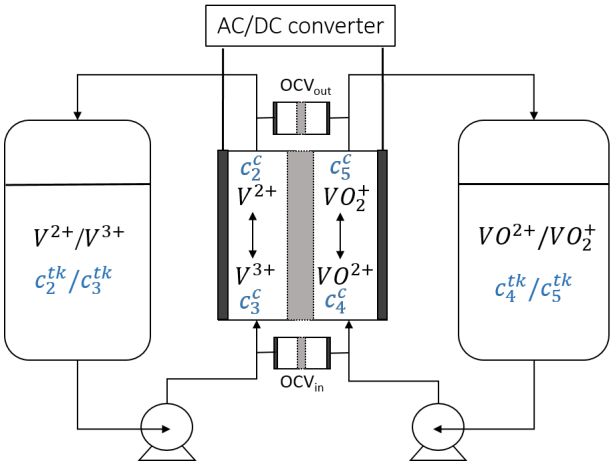

Fig. 1. The configuration of a VRFB system equipped with inlet/outlet open circuit cells

The crossover plays an important role in the dynamics of the system, nevertheless

- its influence on the battery operation within $5-10$ cycles of charge/discharge is negligibly small,
- it can be minimized by choosing proper operating modes,
- presence of the term $\mathcal{J}$ in the model significantly complicates the analysis.

In Section 3 we introduce a simplified dynamical model used to derive a control law.

2.2 Flow Rate Control

The simplest and most common approach for flow rate regulation is to keep it constant. It may seem there is no need for control at all, but since the viscosity of the electrolyte changes over time, the controller is needed even to maintain constant flow rate. However, such an approach lacks flexibility and optimality.

On the one hand, the flow rate should be kept high enough to provide sufficient amount of ions for all possible

fluctuations of loading current. On the other hand, in many cases, the flow rate is significantly higher than it is necessary for the desired battery operation. That in turn, may result in higher losses and higher battery degradation. Therefore, more advanced control strategies are needed.

Faraday's first law of electrolysis determines the minimally required flow rate to maintain the reaction. According to this law, the amount of chemical change being produced by a current at an electrode-electrolyte interface is proportional to the quantity of electricity used, e.g. see Faraday (1834) and Sundén (2019) for the details.

Assuming the electrolyte to be well-balanced, Faraday's law for the flow battery stack with n_c cells can be formulated as

$$u_F = \begin{cases} \dfrac{-n_c w}{F c_b SoC_{tk}} & \text{for discharging, } w < 0, \\ \dfrac{n_c w}{F c_b (1 - SoC_{tk})} & \text{for charging, } w > 0, \end{cases} \tag{9}$$

$$u_F = \begin{cases} \dfrac{-n_c w}{F x_1} & \text{for discharging, } w < 0, \\ \dfrac{n_c w}{F (c_b - x_1)} & \text{for charging, } w > 0, \end{cases}$$

where the state of charge in the tanks is defined as

$$SoC_{tk} = \min\left\{\frac{\xi_1}{c_\mathrm{b}}, \frac{\xi_4}{c_\mathrm{b}}\right\}.$$

The actual flow rate should be higher than u_F given by Faraday's law. Thus, in the literature on this topic, a factor for scaling the flow rate has been introduced. It is commonly referred to as the *flow factor* $\tilde{f}$, e.g. see Tang et al. (2014):

$$u = \tilde{f} \cdot u_F. \tag{10}$$

To formulate the goal of the work, we first introduce the following definition.

Definition 1. The fraction *conversion per pass (or conversion rate)* will be called the parameter determined by the following expression

$$\gamma = \begin{cases} \max\left\{\dfrac{\xi_1 - \xi_5}{\xi_1}, \dfrac{\xi_4 - \xi_8}{\xi_4}\right\} \text{for discharging}, w < 0, \\ \max\left\{\dfrac{\xi_5 - \xi_1}{c_b - \xi_1}, \dfrac{\xi_8 - \xi_4}{c_b - \xi_4}\right\} \text{for charging}, w > 0. \end{cases} \tag{11}$$

The conversion rate equals the amount of active ions participating in the electrochemical reactions during a single-pass of electrolyte through the cell. To ensure a better performance of the battery, the conversion rate is kept low to ensure availability of a sufficient amount of reactants in the cell in case of sudden changes of the loading current. In practice, the manufacturers set it $\approx 5\%$, that provides optimal battery operation under dynamically changing loads, along with good utilization of electrolyte and hence, high battery capacity usage.

The goal of this paper is to demonstrate that the flow factor strategy is in fact a feedback controller aimed to keep the conversion rate around a desired value γ^* and to show, how the flow factor depends on the parameters of the system.

3. MAIN RESULTS

Prior to propose the flow rate controller and analyze its properties, we present a simplified VRFB dynamical model.

3.1 Second-Order Model of VRFB

Let us assume the crossover term to be zero $\mathcal{J} \equiv 0$ and the total concentration of vanadium ions c_b be constant. Observe that we can decrease the dynamic dimension of the system by taking into account its algebraic part, that now takes a different form from (5):

$$\xi_1 + \xi_2 = \xi_3 + \xi_4 = \xi_5 + \xi_6 = \xi_7 + \xi_8 = c_\mathrm{b}, \tag{12}$$

$$\xi_1 = \xi_4,\ \xi_5 = \xi_8. \tag{13}$$

Therefore, introducing new notation $x_1 = \xi_1, x_2 = \xi_5$ system (1) can be reduced to

$$\begin{cases} \dot{x}_1 = (-\alpha x_1 + \alpha x_2)u, \\ \dot{x}_2 = (\beta x_1 - \beta x_2)u + dw. \end{cases} \tag{14}$$

The outputs of system (14) are:

$$y_\mathrm{in} = y_0 + 2y_1 \ln \frac{x_1}{c_\mathrm{b} - x_1}, \tag{15}$$

$$y_\mathrm{out} = y_0 + 2y_1 \ln \frac{x_2}{c_\mathrm{b} - x_2}. \tag{16}$$

Nonlinear transformations give us the exact states of the system:

$$x_1 = \frac{c_\mathrm{b} e^{\frac{y_\mathrm{in} - y_0}{2y_1}}}{1 + e^{\frac{y_\mathrm{in} - c_0}{2y_1}}}, \tag{17}$$

$$x_2 = \frac{c_\mathrm{b} e^{\frac{y_\mathrm{out} - y_0}{2y_1}}}{1 + e^{\frac{y_\mathrm{out} - y_0}{2y_1}}}. \tag{18}$$

From (17) it follows, that having measurements of both OCVs we can easily find the concentrations/SoCs.

In the new notation, equation (11) takes the form

$$\gamma = \begin{cases} \dfrac{x_1 - x_2}{x_1} & \text{for discharging, } w < 0, \\ \dfrac{x_2 - x_1}{c_b - x_1} & \text{for charging, } w > 0. \end{cases} \tag{19}$$

The flow factor based control law (10) is as follows

$$u = \begin{cases} \dfrac{-kw}{x_1} & \text{during discharge, } w < 0, \\ \dfrac{kw}{c_b - x_1} & \text{during charge, } w > 0, \end{cases} \tag{20}$$

where

$$k = \frac{n_c \tilde{f}}{F}.$$

3.2 Understanding the Flow Factor

In this section, we demonstrate that the so-called flow factor control strategy is a special nonlinear feedback

control law aimed to keep a certain value of the conversion rate γ in system (14).

Let us denote a desired conversion rate by $0 < \gamma^* \leq 1$ and suppose the flow rate $u > 0$ to have no upper bound.

Theorem 2. The fraction conversion per pass $\gamma(t)$ of the system asymptotically converges to γ^* for any initial condition $\gamma(0) \in (-\infty,\ 1]$, if the flow rate u follows

$$u = \begin{cases} \dfrac{-kw}{x_1} & \text{during discharge, } w < 0, \\ \dfrac{kw}{c_b - x_1} & \text{during charge, } w > 0, \end{cases}$$

with the flow factor $\tilde{f}$ of the form

$$\tilde{f} = \frac{1}{\gamma^*((1-\gamma^*)\frac{n_c V_c}{V_{tk}} + 1)}.$$

Sketch of the proof. The detailed proof is omitted due to lack of space. The idea of the proof is as follows. First, it is necessary to move from system (14) governed by control law (20) to the dynamics of the conversion rate γ. Further, it can be shown that any value of the desired conversion rate γ^*, that has a physical meaning, is a stable equilibrium of the system. From the expression for the equilibrium, one can also obtain formula (**??**) for flow factor.

Remark 3. Theorem 2 shows that the flow factor can be calculated rather than empirically chosen. It depends on the system stack/tank volumes ratio, the number of cells, and the desired fraction conversion per pass.

Remark 4. The derived control law does not take into account neither boundaries on the control signal, nor boundaries on the states/disturbances. On the one hand, this fact looks limiting and confusing: in this case, in the end of the discharge as $x_1 \to 0$, the flow rate infinitely grows. On the other hand, in practice, the battery storage system operates in the range of SoCs ≈ 0.1 to 0.9, thus never reaching extremely low values of x_1.

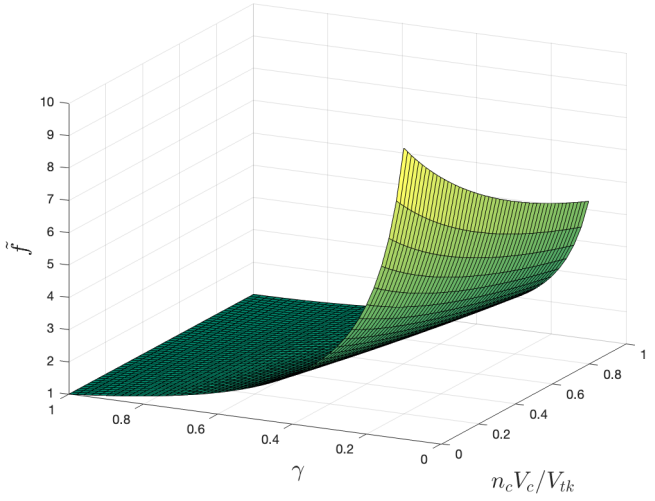

Fig. 2. The behavior of $\tilde{f}$ depending on the volume ratio and conversion rate, $n_c V_c / V_{tk} \in [0,\ 1]$, $\gamma \in [0.1,\ 1]$

It can be seen in Fig. 2 that $\tilde{f}$ starts from unity and tends to infinity, as $\gamma \to 0$. In Fig. 3 we demonstrate the sensitivity of $\tilde{f}$ to the volume ratio for the values that correspond to several real VRFB setups listed in Table 1. Here, "Skoltech-1" and "Skoltech-2" are the VRFB systems located in Skoltech lab, "Padova" is the battery of the University of Padova (see Guarnieri et al. (2019)) and "UNSW" stands for the battery in UNSW (see Tang et al. (2014)).

The results showed that the flow factor for all possible VRFB systems lies in a quite narrow domain between two dashed boundaries. They correspond to the cases when 1) the volume of stack is equal to the volume of tanks (red dashed line) and when 2) the volume of the tanks is significantly greater (black dashed line). Moreover, for the VRFB systems from Table 1, the flow factors are rather similar and located close to the upper boundary. Thus, the flow factor for practical systems is not notably effected by the sizes of the stack and tanks. However, as it can be seen from Fig. 3, the flow factor highly depends on the conversion rate in the cell that is attributed to the fact that for lower conversion the reactants should be refreshed faster, and hence, the flow rate should be higher.

Table 1. Parameters of VRFB setups

VRFB Setup	$V_c,\ m^3$	$V_{tk},\ m^3$	n_c	$\frac{n_c V_c}{V_{tk}}$
Skoltech - 1	7.50e-06	4.00e-04	10	0.1875
Skoltech - 2	1.84e-04	1.00e-01	40	0.0736
Padova	3.42e-04	5.50e-01	40	0.0249
UNSW	4.50e-04	0.2	40	0.0900

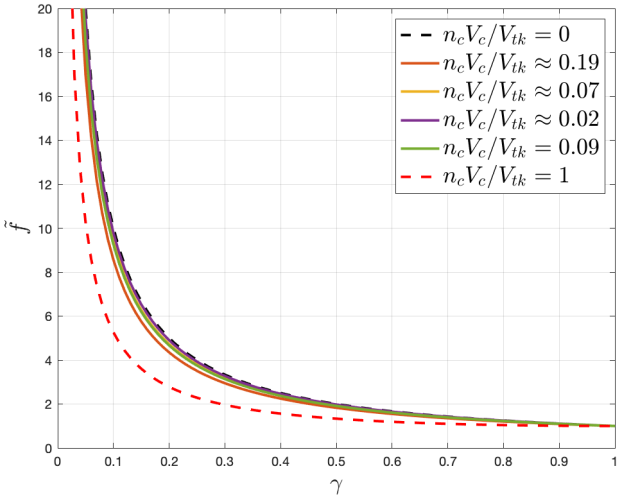

Fig. 3. The plot of $\tilde{f}$ as a function of the conversion rate $\gamma \in [0.05,\ 1]$ for six values of $n_c V_c / V_{tk}$

Next, we present results of simulation of the flow factor control strategy with predefined desired fraction conversion per pass and different initial concentrations of the electrolyte.

4. NUMERICAL SIMULATION

In this section, we demonstrate the performance of the flow factor control strategy and confirm the result of The-

orem 2 through numerical simulations. The simulations were performed for the same loading current profile shown in Fig. 4.

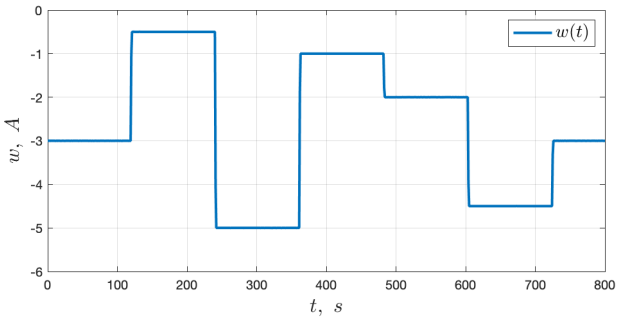

Fig. 4. Loading current $w(t)$ during discharging

The initial concentrations were set as follows:

(1) $x^{(1)}(0) = [1305,\ 1305]^\top$, $SoC_{tk} = 0.9$,
(2) $x^{(2)}(0) = [1035,\ 1305]^\top$, $SoC_{tk} = 0.7$,
(3) $x^{(3)}(0) = [1305,\ 1035]^\top$, $SoC_{tk} = 0.9$.

The parameters of the system were set equal to the parameters of the Skoltech laboratory VRFB setup "Skoltech-1", see Table 1.

The target value of the conversion rate was chosen $\gamma^* = 0.1$. This gives the flow factor $\tilde{f} = 9.2507$.

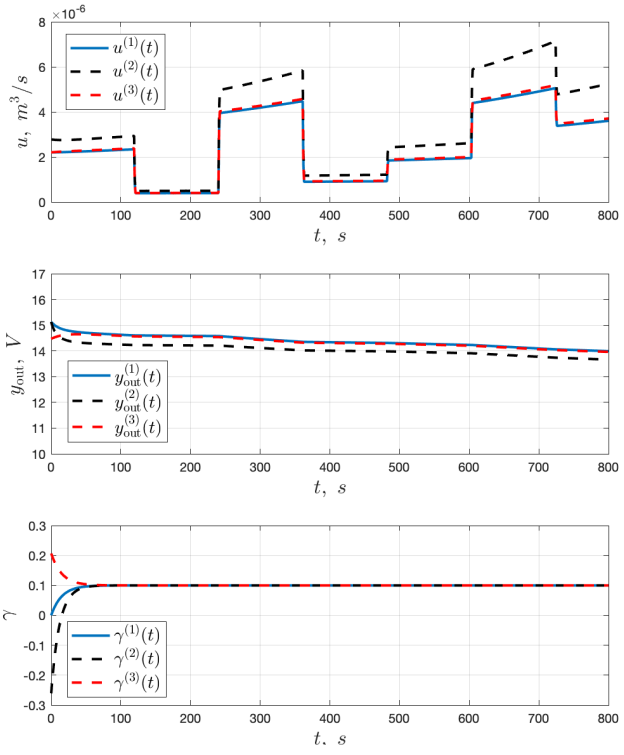

Fig. 5. Evolution of main parameters of the system: flow rate u, outlet OCV y_{out}, and the conversion rate γ for three different initial conditions of x_1 and x_2

The results of the numerical experiment are shown in Fig. 5. The first graph shows the flow rate as a function of time for three initial conditions; the dynamics of corresponding outlet voltages are depicted right after them. Finally, the third graph illustrates the evolution of the conversion rate. According to (19), the first initial condition corresponds to $\gamma(0) = 0$, the second one to $\gamma(0) \approx -0.26$, and the third to $\gamma(0) \approx 0.21$.

As it can be seen in Fig. 5, whatever initial conditions are chosen, the trajectories of $\gamma(t)$ converge to the target value of $\gamma^* = 0.1$. One may notice, that the voltage curve in the second simulation lies lower compared to two other curves. This is explained by the lower initial SoC_{tk}.

5. CONCLUSION

In the paper, we studied the flow factor control strategy. This strategy extends the classical Faraday's law of electrolysis by the use of a special scaling parameter known as the flow factor. In practice, this approach to flow rate regulation involves empirical selection of the flow factor. The paper explains how this parameter is related to the characteristics of the system along with the conversion rate in the battery stack, paving the way for the correct setting of the flow factor prior to perform bench experiments.

The contribution of the paper is threefold. For the VRFB model, we

- performed rigorous analysis of the conversion rate dynamics;
- derived an expression of the flow factor as a function of system parameters (volumes of stack and tanks) and the desired conversion rate. We also analyzed the sensitivity of the flow factor to the target conversion rate and volumes ratio;
- confirmed the theoretical results through numerical simulations.

Our future plans include

- experimental validation of the obtained control law for different target conversion rates;
- design of the control taking into account the boundaries on the states, current and flow rate. Analysis of the settling time and overall performance;
- analysis and minimization of losses.

ACKNOWLEDGEMENTS

This paper is supported by European Union's Horizon 2020 research and innovation programme under grant agreement No 963550, project HyFlow (Hybrid energy storage system).

The authors would like to thank A. Kurilovich and N. Gvozdik (Skoltech, Moscow) for fruitful discussions and interesting suggestions.

REFERENCES

Aneke, M. and Wang, M. (2016). Energy storage technologies and real life applications. A state of the art review. *Applied Energy*, 179, 350–377.

Averbukh, M., Pozin, A., and Sukoriansky, S. (2017). Electrolyte Pumping Optimization in Already Manufactured Vanadium Redox Battery Based on Experimentally Determined Electrical and Hydrodynamic Losses. *Journal of Energy Engineering*, 143(2), 1–12.

Badrinarayanan, R., Tseng, K.J., Soong, B.H., and Wei, Z. (2017). Modelling and control of vanadium redox flow battery for profile based charging applications. *Energy*, 141, 1479–1488.

Blanc, C. and Rufer, A. (2008). Multiphysics and energetic modeling of a vanadium redox flow battery. *2008 IEEE International Conference on Sustainable Energy Technologies, ICSET 2008*, 696–701.

Chen, H., Li, X., Gao, H., Liu, J., Yan, C., and Tang, A. (2019). Numerical modelling and in-depth analysis of multi-stack vanadium flow battery module incorporating transport delay. *Applied Energy*, 247(October 2018), 13–23.

Faraday, M. (1834). Experimental Researches in Electricity. Seventh Series. *Philosophical Transactions of the Royal Society of London*, 124(0), 77–122.

Guarnieri, M., Trovò, A., Marini, G., Sutto, A., and Alotto, P. (2019). High current polarization tests on a 9-kW vanadium redox flow battery. *Journal of Power Sources*, 431(February), 239–249.

Guarnieri, M., Trovò, A., and Picano, F. (2020). Enhancing the efficiency of kW-class vanadium redox flow batteries by flow factor modulation: An experimental method. *Applied Energy*, 262(January), 114532.

Kim, D.K., Yoon, S.J., Lee, J., and Kim, S. (2018). Parametric study and flow rate optimization of all-vanadium redox flow batteries. *Applied Energy*, 228(June), 891–901.

Konig, S., Suriyah, M.R., and Leibfried, T. (2015). Model based examination on influence of stack series connection and pipe diameters on ef fi ciency of vanadium redox fl ow batteries under consideration of shunt currents. *Journal of Power Sources*, 281, 272–284.

Konig, S., Suriyah, M.R., and Leibfried, T. (2016). Innovative model-based flow rate optimization for vanadium redox flow batteries. *Journal of Power Sources*, 333, 134–144.

Largent, R.L., Skyllas-Kazacos, M., and Chieng, J. (1993). Improved PV system performance using vanadium batteries, Conference Record of the Twenty Third IEEE Photovoltaic Specialists Conference. *IEEE*, 1119–1124.

Li, Y., Zhang, X., Bao, J., and Skyllas-Kazacos, M. (2017a). Control of electrolyte flow rate for the vanadium redox flow battery by gain scheduling. *Journal of Energy Storage*, 14, 125–133.

Li, Y., Zhang, X., Bao, J., and Skyllas-kazacos, M. (2017b). Studies on optimal charging conditions for vanadium redox flow batteries. *Journal of Energy Storage*, 11, 191–199.

Ling, C.Y., Cao, H., Chng, M.L., Han, M., and Birgersson, E. (2015). Pulsating electrolyte flow in a full vanadium redox battery. *Journal of Power Sources*, 294, 305–311.

Lucas, A. and Chondrogiannis, S. (2016). Smart grid energy storage controller for frequency regulation and peak shaving , using a vanadium redox flow battery. *International Journal of Electrical Power and Energy Systems*, 80, 26–36.

Pugach, M., Kondratenko, M., Briola, S., and Bischi, A. (2017). Numerical and experimental study of the flow-by cell for Vanadium Redox Batteries. *Energy Procedia*, 142, 3667–3674.

Pugach, M., Kondratenko, M., Briola, S., and Bischi, A. (2018). Zero dimensional dynamic model of vanadium redox fl ow battery cell incorporating all modes of vanadium ions crossover. *Applied Energy*, 226(May), 560–569.

Pugach, M., Parsegov, S., Gryazina, E., and Bischi, A. (2020). Output feedback control of electrolyte flow rate for Vanadium Redox Flow Batteries. *Journal of Power Sources*, 455(February), 227916.

Pugach, M., Vyshinsky, V., and Bischi, A. (2019). Energy efficiency analysis for a kilo-watt class vanadium redox flow battery system. *Applied Energy*, 253.

Shen, H.F., Zhu, X.J., Shao, M., and Cao, H.F. (2013). Neural network predictive control for vanadium redox flow battery. *Journal of Applied Mathematics*, 2013.

Sundén, B. (2019). *Hydrogen, Batteries and Fuel Cells*. Springer.

Tang, A., Bao, J., and Skyllas-Kazacos, M. (2011). Dynamic modelling of the effects of ion diffusion and side reactions on the capacity loss for vanadium redox flow battery. *Journal of Power Sources*, 196(24), 10737–10747.

Tang, A., Bao, J., and Skyllas-Kazacos, M. (2014). Studies on pressure losses and flow rate optimization in vanadium redox flow battery. *Journal of Power Sources*, 248, 154–162.

Trovò, A. (2020). Battery management system for industrial-scale vanadium redox flow batteries: Features and operation. *Journal of Power Sources*, 465(March).

Trovò, A., Guarnieri, M., Engineering, I., and Centre, I. (2021). *Battery Management Systems for Redox Flow Batteries and Controllers for Fuel Cells*. Elsevier Inc.

Viswanathan, V., Crawford, A., Stephenson, D., Kim, S., Wang, W., Li, B., Coffey, G., Thomsen, E., Graff, G., Balducci, P., Kintner-Meyer, M., and Sprenkle, V. (2014). Cost and performance model for redox flow batteries. *Journal of Power Sources*, 247, 1040–1051.

Xiao, W. and Tan, L. (2019). Control strategy optimization of electrolyte flow rate for all vanadium redox flow battery with consideration of pump. *Renewable Energy*, 133, 1445–1454.

Appendix A. PROOF OF THEOREM 1

For the sake of simplicity we consider the discharge mode only, $w < 0$. The results for the charge can be proven in the same way.

The proof is based on the analysis of the behavior of γ and its stability properties with respect to the adjustable parameter k.

Since $u > 0$, let us introduce new time scale in (14), such that

$$d\tau = u^{-1}dt \Rightarrow ud\tau = dt$$

and then change the variables like so:

$$\frac{dx_1}{dt} = -\alpha z, \quad \frac{dz}{dt} = -(\alpha+\beta)z - d\frac{w}{u}, \tag{A.1}$$

where $z = x_1 - x_2$.

Substituting the control signal u by $u = -k\frac{w}{x_1}$, $k > 0$, into (A.1) we find

$$\frac{dx_1}{dt} = -\alpha z, \quad \frac{dz}{dt} = cx_1 - (\alpha+\beta)z, \quad c = d/k. \tag{A.2}$$

The dynamics of (A.2) does not depend neither on u, nor on w. According to (19), $\gamma = z/x_1$, therefore

$$\dot{\gamma} = \frac{\dot{z}}{x_1} - \frac{z\dot{x}_1}{x_1^2},$$

or

$$\dot{\gamma} = c - (\alpha+\beta)\gamma + \alpha\gamma^2. \tag{A.3}$$

Let's find stable equilibria of the last system. The following equation

$$\alpha\gamma^2 - (\alpha+\beta)\gamma + c = 0 \tag{A.4}$$

has the roots:

$$\gamma_{1,2} = \frac{1}{2\alpha}(\alpha+\beta \pm \sqrt{(\alpha+\beta)^2 - 4\alpha c}). \tag{A.5}$$

From the linearized system it follows that we have a pair of stable/unstable fixed points, where a locally stable equilibrium is

$$\gamma = \gamma_1 = \frac{1}{2\alpha}(\alpha+\beta - \sqrt{(\alpha+\beta)^2 - 4\alpha c}) \tag{A.6}$$

provided that

$$(\alpha+\beta)^2 - 4\alpha c > 0, \quad \text{or, equivalently,} \quad c < \frac{(\alpha+\beta)^2}{4\alpha}.$$

Let $V = \frac{1}{2}(\gamma-\gamma_1)^2$ be a Lyapunov function candidate. The set Γ where $V > 0, \dot{V} < 0\ \forall\gamma \in \Gamma$, except for γ_1, where $\dot{V}(\gamma_1) = 0$, is the domain of attraction we are seeking for. Evidently, the function V is positive $\forall\gamma \neq \gamma_1$. It can be shown, that $\frac{dV}{dt} \leq 0\ \forall\gamma \leq \gamma_2$, since $\frac{dV}{dt} = \alpha(\gamma-\gamma_1)^2(\gamma-\gamma_2)$. On the other hand, all the initial conditions $\gamma(0) \geq \gamma_2$ have no physical meaning, due to the fact that $\gamma_2 > 1$. Since $\gamma_1 \leq 1$, we arrive at the condition on k to be satisfied:

$$\begin{gathered}
\sqrt{(\alpha+\beta)^2 - 4\alpha c} \geq \beta - \alpha \\
(\alpha+\beta)^2 - 4\alpha c \geq (\beta-\alpha)^2 \\
\alpha^2 + 2\alpha\beta + \beta^2 - 4\alpha c \geq \beta^2 - 2\alpha\beta + \alpha^2 \\
\beta \geq c \\
k \geq \frac{d}{\beta},
\end{gathered}$$

or equivalently

$$\tilde{f} \geq 1. \tag{A.7}$$

The last inequality illustrates the fact, that the minimal required flow rate is defined by Faraday's law of electrolysis, $\tilde{f} = 1$. Thus, we can conclude, that for any initial condition $\gamma(0) \in (-\infty,\ 1]$ the solution of (A.3) converges to stable equilibrium γ_1 if condition (A.7) is satisfied. Let us now look at system (A.3) and find the flow factor as a function of the target conversion rate γ^*.

Evidently, the stable equilibrium point $\gamma_1 = \gamma^*$ can be found from

$$\gamma^* k((1-\gamma^*)\alpha + \beta) - d = 0,$$

that gives

$$k = \frac{d}{\gamma^*((1-\gamma^*)\alpha+\beta)}.$$

Finally, we find the flow factor $\tilde{f}$ as follows:

$$\tilde{f} = \frac{1}{\gamma^*((1-\gamma^*)\frac{n_c V_c}{V_{tk}} + 1)}.$$

Evidently, for any $\gamma^* \in (0,\ 1]$ the following inequality holds:

$$\tilde{f} \geq 1.$$

This completes the proof.

$$\begin{gathered}
-k\frac{w}{x_1} \leq u_{max} \\
\frac{d}{\beta} < k \leq -u_{max}\frac{x_1}{w}
\end{gathered}$$

Facts and observations:

(1) $0 < c < \frac{(\alpha+\beta)^2}{4\alpha}$ (since $0 < k < \infty$ and the discriminant equal to zero gives unstable equilibrium)
(2) Evolution of $\gamma(t) = \frac{z}{x_1} = -\frac{C_1\lambda_1 e^{\lambda_1 t} + C_2\lambda_2 e^{\lambda_2 t}}{\alpha(C_1 e^{\lambda_1 t} + C_2 e^{\lambda_2 t})}$
(3) $\gamma(0)$ should be $< \gamma_2 = \frac{1}{2\alpha}(\alpha+\beta+\sqrt{(\alpha+\beta)^2 - 4\alpha c})$
(4) Analysis of the admissible initial conditions. Since $\gamma = \frac{x_1 - x_2}{x_1}$ and $x_1, x_2 \in [0,\ c_b]$, then
- $x_1(0) = x_2(0) = c_b$ gives $\gamma(0) = 0$
- $x_1(0) = c_b, x_2(0) = 0$ gives $\gamma(0) = 1$
- $x_1(0) = 0, x_2(0) = c_b$ gives $\gamma(0) = -\infty$
- $x_1(0) = x_2(0) = 0$ gives $\gamma(0) = ?$

Admissible initial conditions for $x_1,\ x_2$

$$\begin{gathered}
x_1(t) = C_1 e^{\lambda_1 t} + C_2 e^{\lambda_2 t}, \\
x_2(t) = C_1(1 + \frac{\lambda_1}{\alpha})e^{\lambda_1 t} + C_2(1 + \frac{\lambda_2}{\alpha})e^{\lambda_2 t}. \\
\lambda_{1,2} = \frac{-(\alpha+\beta) \pm \sqrt{(\alpha+\beta)^2 - 4\alpha c}}{2}, \quad \lambda_1 < \lambda_2 < 0.
\end{gathered}$$

Therefore,

$$\begin{gathered}
x_1(0) = C_1 + C_2, \\
x_2(0) = C_1\rho_1 + C_2\rho_2.
\end{gathered}$$

where

$$\rho_1 = 1 + \frac{\lambda_1}{\alpha} < 0 < \rho_2 = 1 + \frac{\lambda_2}{\alpha}$$

Hence,

$$\begin{gathered}
C_1 = \frac{\rho_2 x_1(0) - x_2(0)}{\rho_2 - \rho_1} \\
C_2 = \frac{x_2(0) - \rho_1 x_1(0)}{\rho_2 - \rho_1}.
\end{gathered}$$

$$\begin{aligned}
x_1(t) &= \frac{(\rho_2 e^{\lambda_1 t} - \rho_1 e^{\lambda_2 t})x_1(0) + (e^{\lambda_2 t} - e^{\lambda_1 t})x_2(0)}{\rho_2 - \rho_1} \\
&\leq e^{\lambda_2 t}x_1(0) + \frac{1}{\rho_2 - \rho_1}e^{\lambda_1 t}x_2(0)
\end{aligned}$$

$$\begin{aligned}
x_2(t) &= \frac{\rho_1\rho_2(e^{\lambda_1 t} - e^{\lambda_2 t})x_1(0) + (\rho_2 e^{\lambda_2 t} - \rho_1 e^{\lambda_2 t})x_2(0)}{\rho_2 - \rho_1} \\
&\leq \frac{(-\rho_1\rho_2)}{\rho_2 - \rho_1}e^{\lambda_2 t}x_1(0) + e^{\lambda_2 t}x_2(0)
\end{aligned}$$

Hence, if

$$x_1(0) + \frac{1}{\rho_2 - \rho_1}x_2(0) \leq c_b \text{ and } \frac{(-\rho_1\rho_2)}{\rho_2 - \rho_1}x_1(0) + x_2(0) \leq c_b$$

then $x_1(t) \leq c_b$ and $x_2(t) \leq c_b$ for all $t \geq 0$.

From the last two equations we get

$$\begin{gathered}
C_1 = \frac{-\alpha x_2(0) + (-\beta + \sqrt{(\alpha+\beta)^2 - 4\alpha c})x_1(0)}{2\sqrt{(\alpha+\beta)^2 - 4\alpha c}}, \\
C_2 = \frac{\alpha x_2(0) - (-\beta - \sqrt{(\alpha+\beta)^2 - 4\alpha c})x_1(0)}{2\sqrt{(\alpha+\beta)^2 - 4\alpha c}}
\end{gathered}$$

The trajectories have the form:

$$x_1(t) = \frac{-\alpha x_2(0) + (-\beta + \sqrt{(\alpha+\beta)^2 - 4\alpha c})x_1(0)}{2\sqrt{(\alpha+\beta)^2 - 4\alpha c}} e^{\lambda_1 t} + \\ + \frac{\alpha x_2(0) - (-\beta - \sqrt{(\alpha+\beta)^2 - 4\alpha c})x_1(0)}{2\sqrt{(\alpha+\beta)^2 - 4\alpha c}} e^{\lambda_2 t},$$

denote $H = \sqrt{(\alpha+\beta)^2 - 4\alpha c}$,

$$x_2(t) = \frac{-\alpha(-\beta - H)x_2(0) + (\beta^2 - (\alpha+\beta)^2 + 4\alpha c)x_1(0)}{2\alpha H} e^{\lambda_1 t} \\ + \frac{\alpha(-\beta + H)x_2(0) - (\beta^2 - (\alpha+\beta)^2 + 4\alpha c)x_1(0)}{2\alpha H} e^{\lambda_2 t}$$

Since during the discharge the relation $\frac{x_1 - x_2}{x_1} = \gamma$ should hold, we can use this expression to derive the flow rate u. Thus,

$$\dot{x}_1 = -\gamma\alpha u x_1,$$
$$(1-\gamma)\dot{x}_1 = \gamma\beta u x_1 + dw.$$

From last two equations it follows that

$$u = -\frac{n_c \beta w}{\gamma((1-\gamma)\alpha + \beta)x_1}.$$

For the case of charge we have: $\frac{c_b - x_1 - c_b + x_2}{c_b - x_1} = \gamma$. Similarly to the previous case, we get

$$u = \frac{n_c \beta w}{\gamma((1-\gamma)\alpha + \beta)(c_b - x_1)}.$$

The flow factor can be easily found.

In the next section, we demonstrate how the dynamical model may help if one of the measurements is missing or needs to be doublechecked.

A.1 Classic Coulomb Counting Method and Proper SoC Estimation

System (14) can be decomposed into two subsystems due to the properties of matrix A (**??**). The eigenvalues of A and corresponding eigenvectors are

$$\lambda_1 = 0, \quad \nu_1 = [1,\ 1]^\top, \tag{A.8}$$
$$\lambda_2 = -(\alpha+\beta), \quad \nu_2 = [1,\ -\frac{\beta}{\alpha}]^\top. \tag{A.9}$$

Let us introduce new state variables

$$\tilde{x} = S^{-1}x, \tag{A.10}$$

where S is a new basis of eigenvectors

$$S = \begin{bmatrix} 1 & 1 \\ 1 & -\frac{\beta}{\alpha} \end{bmatrix} = \begin{bmatrix} 1 & 1 \\ 1 & -\frac{V_{tk}}{n_c V_c} \end{bmatrix}. \tag{A.11}$$

Then, the dynamics in new coordinates can be rewritten as

$$\dot{\tilde{x}} = u\Lambda\tilde{x} + \tilde{D}w, \tag{A.12}$$

with

$$\Lambda = \begin{bmatrix} 0 & 0 \\ 0 & -(\alpha+\beta) \end{bmatrix}, \tag{A.13}$$
$$\tilde{D} = \begin{bmatrix} \tilde{d} & -\tilde{d} \end{bmatrix}^\top, \tag{A.14}$$

where

$$\tilde{d} = \frac{\alpha d}{\alpha+\beta} = \frac{n_c}{F(n_c V_c + V_{tk})}$$

Let us find out what this coordinate transformation means. Transformation (A.10) writes as

$$\begin{bmatrix} \tilde{x}_1 \\ \tilde{x}_2 \end{bmatrix} = \frac{1}{V_{tk} + n_c V_c} \begin{bmatrix} V_{tk} & n_c V_c \\ n_c V_c & -n_c V_c \end{bmatrix} \begin{bmatrix} x_1 \\ x_2 \end{bmatrix}. \tag{A.15}$$

Thus, $\tilde{x}_1$ can be treated as ********, while $\tilde{x}_2$ is a .... **** ADD

The dynamics are

$$\begin{bmatrix} \dot{\tilde{x}}_1 \\ \dot{\tilde{x}}_2 \end{bmatrix} = u \begin{bmatrix} 0 & 0 \\ 0 & -(\frac{1}{V_{tk}} + \frac{1}{n_c V_c}) \end{bmatrix} \begin{bmatrix} \tilde{x}_1 \\ \tilde{x}_2 \end{bmatrix} + \begin{bmatrix} \frac{n_c}{F(V_{tk} + n_c V_c)} \\ -\frac{n_c}{F(V_{tk} + n_c V_c)} \end{bmatrix} w. \tag{A.16}$$

The variable $\tilde{x}_1$ depends on the current and its initial state:

$$\tilde{x}_1 = \tilde{x}_1(0) + \frac{n_c}{F(V_{tk} + n_c V_c)} \int_0^t w(\tau) d\tau, \tag{A.17}$$

or in the original coordinates

$$V_{tk} x_1 + n_c V_c x_2 = V_{tk} x_1(0) + n_c V_c x_2(0) + \frac{n_c}{F} \int_0^t w(\tau) d\tau. \tag{A.18}$$

In some approaches, this counter is considered in a simplified form, the part related to the stack is neglected. This may lead to incorrect results if the volume of the stack is not negligibly small as compared to the tank's volume. For instance, such a situation is typical for lab-scale benches.